ORIGINAL RESEARCH

Preparation and liquid crystal phase properties of discotic cellulose nanoparticles

Chenxi Li · Julian Evans · Nan Wang · Tingbiao Guo · Sailing He

Abstract Understanding the behavior of fluids with inhomogeneous structural properties is critical for many industrial and biological materials. Sulfuric acid hydrolysis of cotton with ultrasonic treatment and low-speed centrifugation during purification yields "spiky" discotic cellulose particles. Amorphous cellulose remained in solution and forms discotic units which may be nucleated by crystalline rods. Scanning electron microscope and transmission electron microscope images confirm the discotic nature of the cellulose. High speed centrifugation could recover rod-like cellulose nanocrystals from the discotic cellulose nanoparticle solution. 3.6 wt% discotic cellulose nanoparticles formed the typical nematic phase and the liquid crystal texture became more structured with increasing concentration. Our results showed that spontaneous structuring of amorphous cellulose can lead to phase behavior that cannot be achieved using just rod-like cellulose nanocrystals.

Chenxi Li and Julian Evans contributed equally to this manuscript.

C. Li · J. Evans · N. Wang · T. Guo · S. He
Centre for Optical and Electromagnetic Research, Zhejiang University, Hangzhou 310058, China

C. Li · J. Evans (✉) · N. Wang · T. Guo · S. He (✉)
Department of Electromagnetic Engineering, Royal Institute of Technology, 100 44 Stockholm, Sweden
e-mail: juliane@colorado.edu

S. He
e-mail: sailing@zju.edu.cn

Graphic abstract Mixtures containing amorphous and crystalline cellulose can form discotic cellulose nanoparticles. These solutions can form nematic phase (**A**), a structured columnar-like phase (**B**), and a glassy phase (**C**). Scanning electron microscope characterization (**D**, **E**) confirms a discotic structure with some spikes and network formation
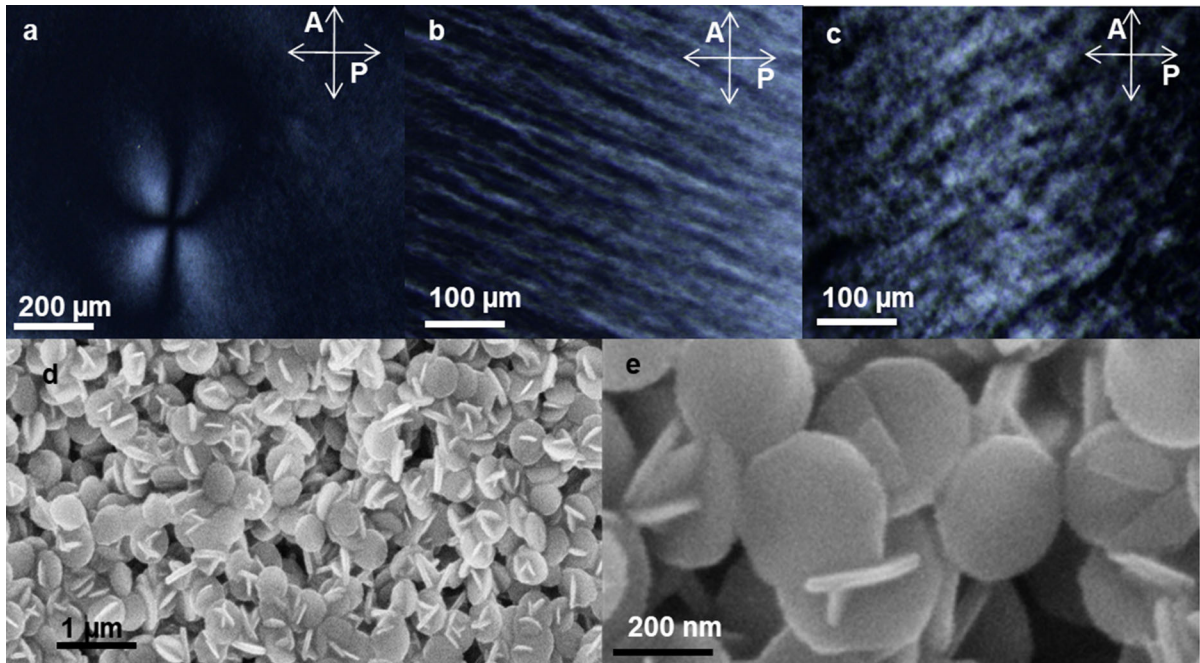
Keywords Discotic cellulose nanoparticles · Liquid crystals · Phase behaviors

Introduction

Native cellulose consists of rod-like crystalline regions and amorphous regions with cavities and defects (Habibi et al. 2010), where amorphous regions are more easily attacked by acid (Lagerwall et al. 2014). Traditional acid hydrolysis and purification methods can remove amorphous regions completely and leave rod-like crystalline regions (Moon et al. 2011), producing rod-like cellulose nanocrystals (CNCs) that have a typical size around 5–20 nm thick and 100–500 nm long (Elazzouzi-Hafraoui et al. 2008; Schütz et al. 2015). CNCs typically form chiral nematic phase liquid crystals (LCs) at a critical concentration with a pitch on the order of microns or tens of microns (Parker et al. 2018; Shafiei-Sabet et al. 2014). Nematic phase is achievable with high aspect ratio bacterial cellulose (Araki and Kuga 2001) and plant-based cellulose at pH around 1 or above 10 (Li et al. 2019; Liu et al. 2014). While an incomplete removal of amorphous cellulose can produce a mixture of shape polydispersity and reduced crystallinity, previous reports claimed the preparation of "spherical cellulose nanocrystals (SCNCs)" and formed nematic phase LCs at the concentration of 3.9%, whose phase texture changed with increasing concentration of SCNCs (Wang et al. 2008). Here we observed the "spiky discotic cellulose nanoparticle" after mild acid hydrolysis of cellulose and ultrasonic treatment several hours. Discotic nanoparticles or molecules form nematic and columnar phases upon increasing the

concentration of plates as entropic steric interactions (Bates and Frenkel 1998; Veerman and Frenkel 1992). Discotic LCs can form a different set of phases than rod-like mesogens due to the natural packing of discs (Wöhrle et al. 2016). Understanding the process of producing discotic cellulose with lower crystallinity expands the toolbox of cellulose based solutions and films.

In the present work, discotic cellulose nanoparticles (DCNPs) were prepared by mild sulfuric acid hydrolysis and sonication for 10 min in each hour of the reaction. After high speed centrifugation, the amorphous cellulose could be removed and the DCNPs solution would change to typical rod-like CNCs. Scanning electron microscopy (SEM), transmission electron microscopy (TEM), Raman spectrometer and X-ray diffractometer (XRD) were used to further characterize DCNPs and rod-like CNCs. Phase behaviors of DCNP LCs were observed under the polarized optical microscopy (POM) both in bulk and droplets surrounded by silicone oil. Phase properties of DCNP LCs were analyzed by small X-ray scattering (SAXS).

Results and discussion

In the typical acid hydrolysis method on native cellulose, rod-like CNCs can be obtained in less than 1 h with complete removal of the amorphous cellulose (Beck-Candanedo et al. 2005; Chen et al. 2015). From our experiment, the acid-cellulose mixture was under ultrasonic treatment 10 min during each hour of acid hydrolysis in a water bath, where the reaction proceeded for 3 h in 63.7 wt% acid with a lower reaction rate. It is in accordance with the preparation of SCNCs by mild acid hydrolysis under ultrasonic treatment for 10 h (Wang et al. 2008). Without ultrasonic treatment, the sulfuric acid would react with the surface cellulose first and then permeate into the inside cellulose fiber, while ultrasonic treatment rapidly injects the acid into the inside amorphous regions leading to the formation of submicrometer fragments (Wang et al. 2008). Ultrasonic treatment during hydrolysis and low speed centrifugation during purification are critical in preparing DCNPs.

These cellulose mixtures after hydrolysis are observed under the SEM, and show a "spiky discotic" appearance (Fig. 1a). TEM images of DCNPs shown in Fig. 1b present the circular structures, illustrating

the discotic shape of the nanoparticles, whose size distributions are characterized by the dynamic light scatter (DLS) meter in Fig. 1e that exhibits relatively normal with diameters ranging from 150 to 400 nm. With increasing the reaction time, the diameter of DCNPs is decreased and the smallest diameter is around 100 nm after hydrolysis for 10 h. Adding alkaline solution or high speed centrifugation would destroy the discotic structures, resulting in a solution of rod-like CNCs (Fig. 1c, d). From normalized Raman spectra of DCNPs and CNCs in the frequency range from 850 to 1250 cm^{-1} (Fig. 1f), DCNPs have a peak around 1096 cm^{-1} characteristic of the Glucoside bond (C–O–C) of cellulose skeletons, while CNCs have a peak at 996 cm^{-1} with corresponds to the bending vibrations of CH_2 groups (Chiriu et al. 2018) and a smaller peak at 1096 cm^{-1}, indicating more glucopyranose presented in DCNPs. X-ray diffraction (XRD) patterns of DCNPs and CNCs (Fig. 1g) present almost identical patterns while DCNPs show significantly reduced intensity and broader width, illustrating DCNPs have a lower crystallinity than CNCs. The crystallinity index (C_r) is calculated from XRD data as:

$$C_r = \frac{I_{200} - I_{am}}{I_{200}}, \tag{1}$$

where I_{200} presents the diffraction intensity of the crystalline peak (200) of the maximum when diffraction angle 2θ between 22° and 23°, and I_{am} is the amorphous donated intensity for the minimum at 2θ between 18° and 19° (Jin et al. 2015; Segal et al. 1959). The crystallinity index of DCNPs calculated from measured XRD pattern is $C_{r,DCNPs} \approx 0.79$, and corresponding crystallinity index of CNCs is $C_{r,CNCs} \approx 0.83$, indicating there are more amorphous components existed in DCNPs.

The formation process of DCNPs is shown in Fig. 2. After being hydrolyzed for 1 h, the cellulose in solution forms a network of interconnected discs with large blobs visible (Fig. 2a). For 2 h of hydrolysis the sample still shows large amounts of interconnection with no large blobs (Fig. 2b). With increasing the reaction time to 3 h, samples show relatively uniform and reasonably well-separated circular discotic structures (Fig. 2c, d). Since there are rod-like crystals embedded in the disc structures, a plausible mechanism of formation nucleation by the CNCs and redeposition of amorphous cellulose in the discotic
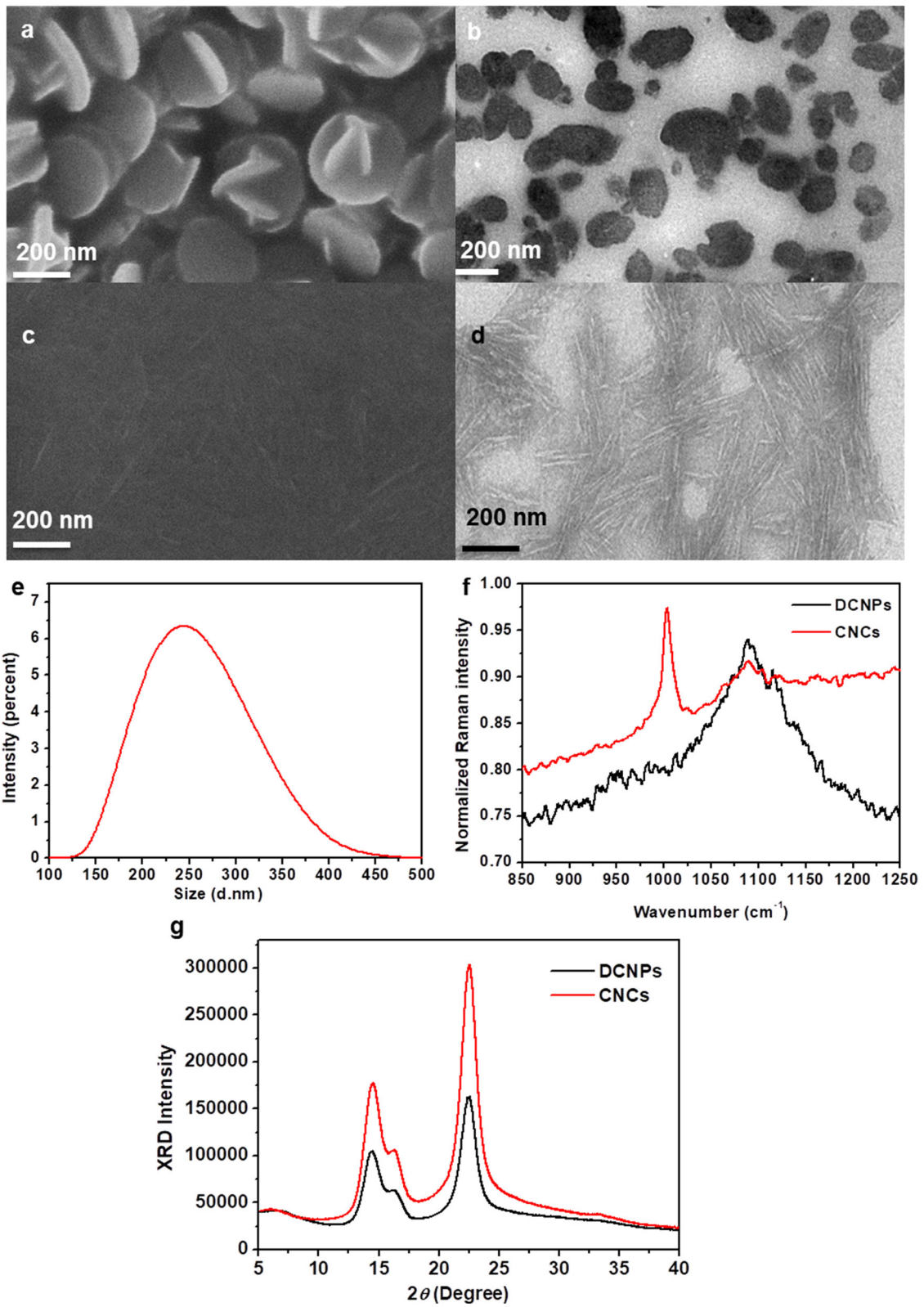
◄**Fig. 1** SEM (**a**) and TEM (**b**) pictures of DCNPs. SEM and TEM images of CNCs are shown in (**c**) and (**d**) respectively. **e** Size distribution of 0.5 wt% DCNP suspensions measured by the DLS meter. **f** Normalized Raman spectra of DCNPs (black line) and CNCs (red line) in the frequency range 850–1250 cm^{-1} measured from the Raman spectrometer. **g** XRD pattern of DCNPs (black line) and CNCs (red line) tested by the X-ray diffractometer with 2θ ranging from 5° to 40°

shape around the CNC as schematically shown in Fig. 2e. Since we are only able to observe the nanoscale behavior in dried samples it is also possible that the discotic units and CNCs are independent in the low pH solution. The relationship between CNCs and discs in the DCNP solution remains an open question.

DCNPs could form different LC textures depending on the concentration as shown in Fig. 3. Encapsulating

DCNP LCs in silicone oil forms DCNP-silicone oil droplets, allowing for the real-time study of phase behaviors of DCNP LCs. Silicone oil plays no noticeable role in the phase behavior itself, and DCNP LC phase behaviors discussed here can be observed in the bulk with no silicone oil present (Fig. 3a, d, g) or the droplet form (Fig. 3c, f, i) at same conditions when diameters of cellulose-silicone droplets are on the order of 100 μm (Li et al. 2016). From our results, 3.6 wt% DCNP suspensions form the nematic phase, showing a typical Schlieren texture with integer strength defects (Fig. 3a, b, c,). With a concentration of 7 wt%, the banded texture is observed in both bulk (Fig. 3d, e) and droplet forms (Fig. 3f). This banded texture was similar to the previous report about the SCNC system at higher concentrations (Wang et al. 2008) while did not provide an explanation of the

Fig. 2 SEM images of discotic cellulose particles that have been hydrolyzed for 1 h (**a**) and 2 h (**b**). Increasing hydrolyzing reaction time to 3 h, there presents nanoparticles with clear disc shapes (**c**, **d**). A plausible mechanism of nucleation and redeposition is schematically depicted in (**e**)
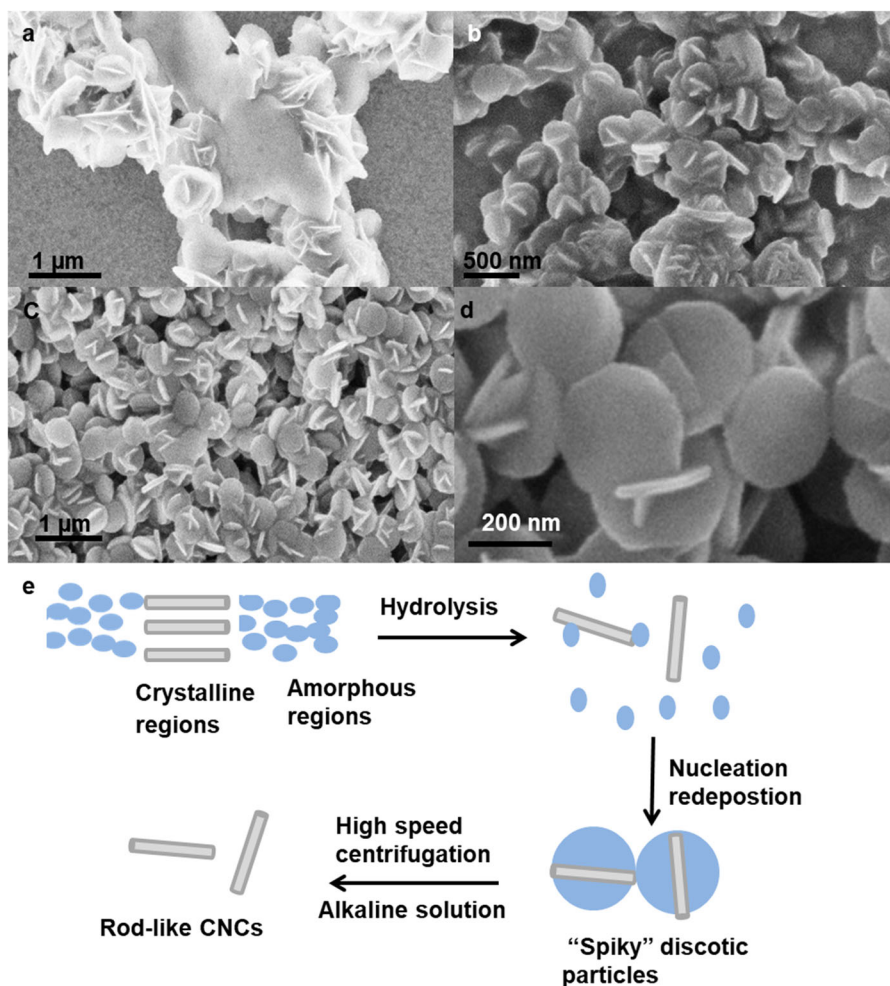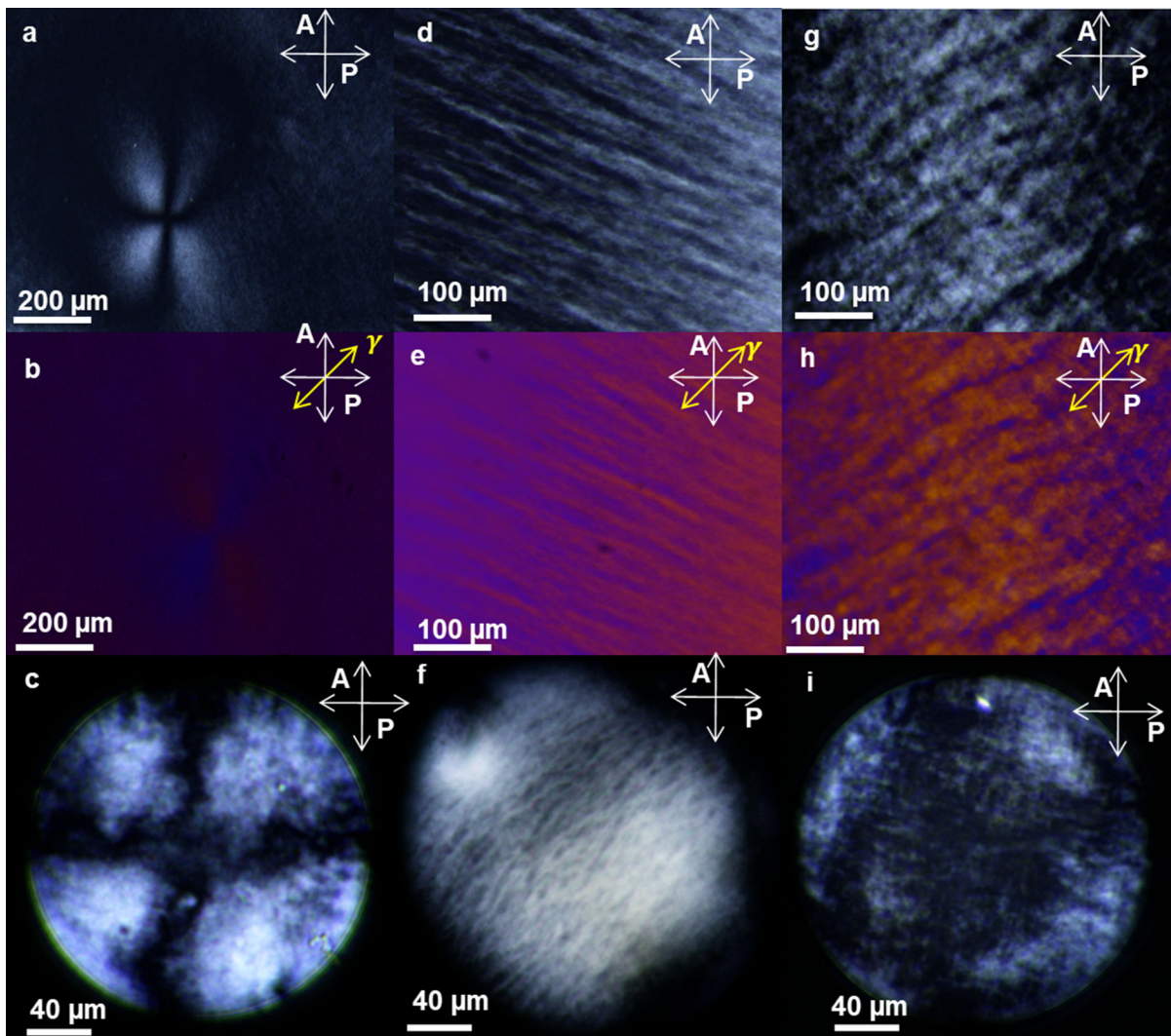
Fig. 3 POM images of 3.6 wt % DCNP LCs in the bulk (**a**), and (**b**) with a phase compensator (530 nm λ-plate) and (**c**) in a droplet surrounded by silicone oil; POM images of 7 wt% DCNP LCs in the bulk (**d**), and (**e**) with a phase compensator (530 nm λ-plate) and (**f**) in a droplet surrounded by silicone oil; POM images of 17 wt% of DCNP mixtures in the bulk (**g**), and (**h**) with a phase compensator (530 nm λ-plate) and (**i**) in a droplet surrounded by silicone oil. *P* and *A* present the polarization directions of the polarizer and the analyzer and γ exhibits the slow axis of the λ-plate

phase behavior. This banded texture LC never produced iridescent color in dried films consistent with no chirality being actively expressed in the phase. The banded texture is typically associated with columnar phase that do not form macroscopic geometrical domains (Martin et al. 2006). The organization of this banded texture LC sample within a droplet is the striped-ball configuration that is consistent with a columnar phase since bending is the only allowed deformation (Fig. 3f). Increasing the DCNP concentration up to 17 wt%, the discotic cellulose LCs

mixture become highly viscous without flow, showing a crosshatch texture in both bulk (Fig. 3g) and droplet (Fig. 3h) configurations. This crosshatch texture is clearly distinct from the Schlieren and fingerprint texture of nematic and chiral nematic phase respectively. In the crosshatch texture POM image with full-wavelength (530 nm) retardation plate (Fig. 3i), this crosshatch texture consists of many smaller domains showing a particular birefringence. This is similar to the reported "birefringent glassy phase" for post-sulfated cellulose fluids (Araki et al. 2000) and

boehmite suspensions (Buining et al. 1994). Concentration of DCNPs is critical in controlling phase behaviors and properties of DCNP LC systems.

DCNPs form nematic phase and more structured LC textures with increasing DCNPs concentration, where the phase behavior is governed by entropic steric interactions that minimize excluded volume (Veerman and Frenkel 1992). Rod-like CNC systems, CNCs could form chiral nematic and nematic phases which are consistent with Stroobants–Lekkerkerker–Odijk (SLO) theory (Li et al. 2019; Stroobants et al. 1986). CNCs formed nematic phase at concentrations ranging from 3 to 20% (Liu et al. 2014), while DNCPs formed banded texture LCs when the concentration above 6 wt%. The behavior of the 7 wt% DCNP LCs with banded texture (inset in Fig. 4a) is further analyzed by small angle X-Ray scattering(SAXS)

and compared with 3.6 wt% DCNP and 7 wt% CNC nematic LCs presenting Schlieren texture (insets in Fig. 4b, c). The scattering intensity of 7 wt% DCNP LCs is around 60 times (Fig. 4a) stronger than 3.6 wt% DCNP LCs (Fig. 4b), and 24 times for 7 wt% CNC nematic LCs (Fig. 4c), indicating some lattice-like behavior that generates a dramatic increase in scattering intensity. From Fig. 4d, 3.6 wt% and 7 wt% DCNP LCs both have a peak at q below 0.1, where 3.6 wt% DCNPs LCs (black line with squares) have a single peak with no shoulder while 7 wt% DCNP LCs (red line with circles) have a single peak with a shoulder, suggesting there is not a regular lattice that supports multiple modes but could be an irregular lattice that produces the shoulder effect. The rod-like crystallites are embedded within the discotic structures with relatively random orientation and add significantly to
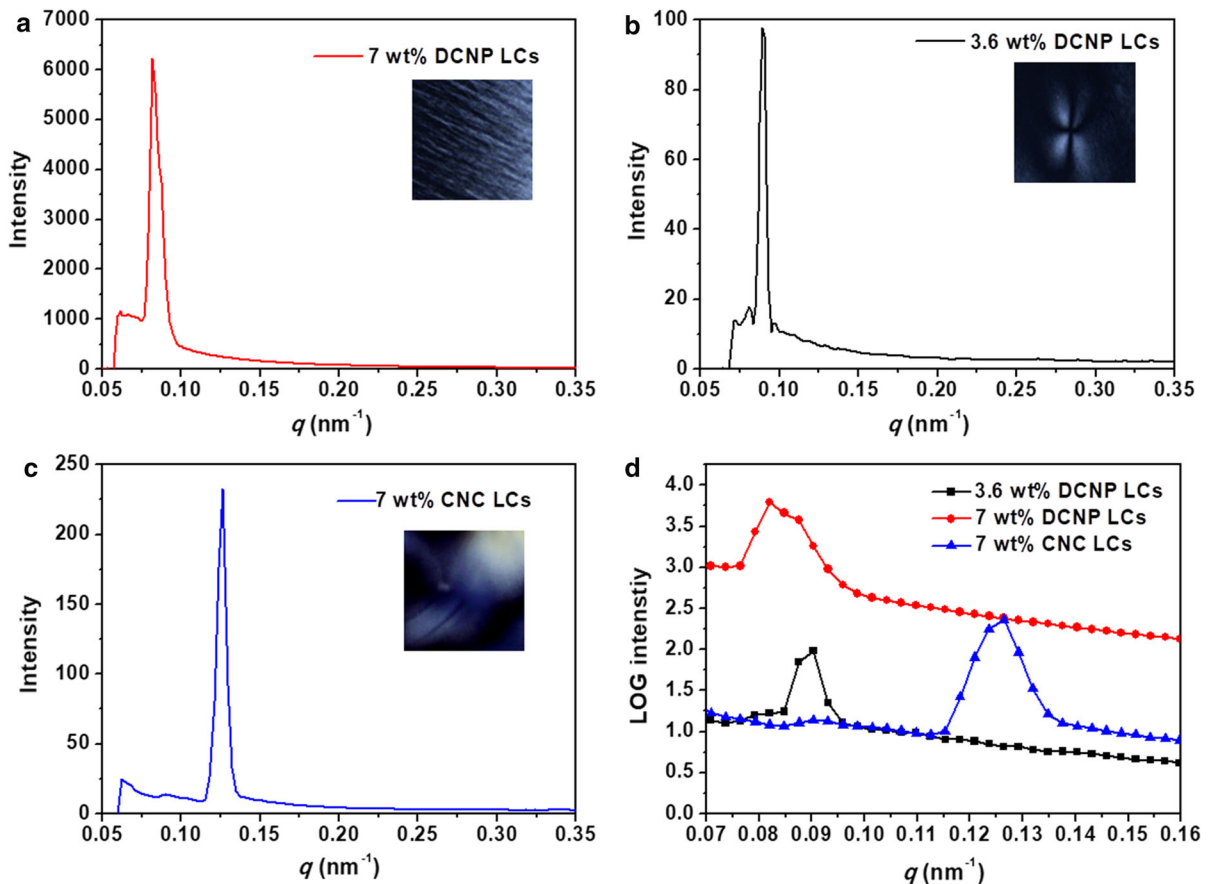

Fig. 4 **a** SAXS pattern of 7 wt% DCNP LCs (red line) which exhibits banded texture in POM imaging (inset); **b** SAXS patterns for 3.6 wt% DCNP LCs (black line) which exhibits Schlieren texture in POM imaging (inset); **c** SAXS patterns of 7 wt% CNC LCs (blue line) which exhibits Schlieren texture in POM imaging (inset), The major peak is magnified and plotted with a log scale in (**d**)

the disorder of this phase. 7 wt% CNC nematic LCs (blue line with triangles) have a single peak for q_c around 0.13 nm^{-1} which is significantly red-shifted from DCNP LCs peak at $q_D = 0.08$ nm^{-1}, illustrating that the spacing in DCNP systems is larger than in CNC mixtures. Discs are well-known to form columns while rod-like CNCs prefer to form parallel and perpendicular twist orientation, indicating the shape of nanoparticles is critical in phase behaviors and properties. DCNP solutions show many features consistent with columnar-like phases. Different phase behaviors and properties of DCNP and CNC systems are due to the structure–property relationships (Wöhrle et al. 2016).

Conclusion

Discotic cellulose nanoparticles from the digestion of cotton with low centrifugation speed and ultrasonic treatment were observed, in which the amorphous cellulose formed discotic particles with spikiness associated with CNCs. Discotic cellulose nanoparticles exhibited the typical nematic phase at the concentration of 3.6 wt% and showed the "banded texture" with increasing concentration to 7 wt%, while discotic cellulose mixtures became glassy states when the concentration above 20 wt%. Careful observation of phase behaviors of discotic cellulose nanoparticles solutions shows that entropic steric interactions and minimize excluded volume effects are critical in phase properties. The preparation and formation of discotic cellulose nanoparticles will inspire the production of different shape cellulose nanoparticles. The character of discotic cellulose nanoparticles forming liquid crystals may give an application in functional and templated materials.

Materials and methods

Preparation discotic cellulose nanoparticles

7 g of degreasing cotton was dispersed in 140 mL of 63.7% sulfuric acid and stirred at 46 °C in a water bath for 3 h. The mixture was sonicated for 10 min during each hour of the hydrolysis reaction. The Sonicator KQ-600DE (Kunshan ultrasonic instrument, China)

was used with an output power around 600 W and a frequency of 40 kHz. 150 mL of deionized water was added to the resulting dispersion to quench the acid hydrolysis process. Cellulose mixtures in 1.5 mL tubes were then centrifuged at 5000 rpm for 10 min three times to remove redundant acid and form LCs. Centrifugation above 7000 rpm for 30 min or adding 2 μL 1 mol/L NaOH into 10 mL 1.5 wt% DCNP suspensions recovered the rod-like CNCs from the DCNP solution. Size distributions of discotic nanoparticles for a 0.5 wt% solution were measured by dynamic light scattering meter using a Zano ZS (Malven, United Kingdom) at room temperature.

Electron microscope imaging

After each sonication, 3 mL of the mixture was removed and diluted to 1.5 wt%. 30 μL 1.5 wt% cellulose dispersions were deposited on indium tin oxide (ITO) glass by spin-coating at 6500 rpm for 59 s and dried at room temperature for 24 h. SEM images of these cellulose specimens were obtained using the Raith 150 TWO (Raith GabH, Germany) under InLens mode with an accelerating voltage of 5 kV. Diluted DCNPs suspensions of 0.017 wt% were dropped on the one side of copper grids, and a filter paper was added on the other side of copper grids to absorb surplus acid fluid, where the dried cellulose samples were observed under transmission electron microscopy JEM-1200 (JEOL, Japan). The CNCs were obtained by high speed centrifugation of the DCNP solution at 7000 rpm for 30 min and dilution to 1.5 wt% and then observed under the Raith 150 TWO. The TEM image of rod-like CNCs was negatively stained with uranyl acetate first and then observed under the JEM-1200.

Spectral characterization and X-ray scattering

7 wt% DCNP and CNC suspensions were dropped on glass substrates and dried at room temperature for 24 h to obtain the samples for Raman spectral characterization. The Raman spectrometer, Lab HR800 (JDbin Yvon, France), measured within a range of wavenumber from 100 to 4000 cm^{-1} with the resolution of 1 cm^{-1} using a 514 nm Ar laser with an output power around 3.5 mW focused on the surface of samples. 7 wt% DCNP and CNC suspensions were coated on the surface of glass substrates (2 cm × 2 cm) and dried at

room temperature for 24 h to produce the XRD samples. We used an X-ray diffractometer Gemini A OHra (Oxford (Valian), Britain) to measure the XRD patterns of DCNPs and CNCs, with an output voltage of 40 kV and current of 30 mA with X-rays from a Cu target ($\lambda = 0.154184$ nm) and measured 2θ ranging from 5° to 40°.

Phase behaviors and properties

POM images of DCNP LCs in the bulk and droplet boundaries were taken using the optical microscope (Olympus BX-53 M). DCNP LC droplets were obtained by dispersing DCNP LCs into silicone oil and stirred for several minutes until homogeneously mixing to get relatively uniform LC droplets surrounded by silicone oil with diameter larger than 100 μm. DCNP suspensions were diluted with deionized water or evaporated in the atmosphere environment to make the desired cellulose concentration. Concentrations of DCNP suspensions were determined as follows: a 200μL discotic cellulose suspension was weighed under an analytical balance, followed by drying at 40 °C for 48 h to remove the solvent completely and weighed again. Small angle X-ray scattering using a SAXS/WAXS SYSTEM (XENOCS, France) further characterized the phase properties of DCNP banded texture LC with 7 wt%, 3.6 wt% DCNP and 7 wt% CNC nematic LCs. 7 wt% CNC nematic LCs prepared by decreasing the pH below 1.5 (Li et al. 2019). An X-ray with a wavelength of 0.15418 nm and an output voltage of 50 kV and current of 0.6 mA travelled through the sample in a capillary glass tube. The scattering intensities were recorded by the detector 2.5 m behind the sample.

References

Araki J, Kuga S (2001) Effect of trace electrolyte on liquid crystal type of cellulose microcrystals. Langmuir 17:4493–4496

Araki J, Wada M, Kuga S, Okano T (2000) Birefringent glassy phase of a cellulose microcrystal suspension. Langmuir 16:2413–2415

Bates MA, Frenkel D (1998) Infinitely thin disks exhibit a first order nematic-columnar phase transition. Phys Rev E 57:4824–4826

Beck-Candanedo S, Roman M, Gray DG (2005) Effect of reaction conditions on the properties and behavior of wood cellulose nanocrystal suspensions. Biomacromol 6:1048–1054

Buining P, Philipse A, Lekkerkerker H (1994) Phase behavior of aqueous dispersions of colloidal boehmite rods. Langmuir: ACS J Surf Colloids 10:2106–2114

Chen L, Wang Q, Hirth K, Baez C, Agarwal UP, Zhu JY (2015) Tailoring the yield and characteristics of wood cellulose nanocrystals (CNC) using concentrated acid hydrolysis. Cellulose 22:1753–1762

Chiriu D, Ricci PC, Cappellini G, Salis M, Loddo G, Carbonaro CM (2018) Ageing of ancient paper: a kinetic model of cellulose degradation from Raman spectra. J Raman Spectrosc 49:1802–1811

Elazzouzi-Hafraoui S, Nishiyama Y, Putaux J-L, Heux L, Dubreuil F, Rochas C (2008) The shape and size distribution of crystalline nanoparticles prepared by acid hydrolysis of native cellulose. Biomacromolecules 9:57–65

Habibi Y, Lucia LA, Rojas OJ (2010) Cellulose nanocrystals: chemistry, self-assembly, and applications. Chem Rev 110:3479–3500

Jin L, Li W, Xu Q, Sun Q (2015) Amino-functionalized nanocrystalline cellulose as an adsorbent for anionic dyes. Cellulose 22:2443–2456

Lagerwall JPF, Schütz C, Salajkova M, Noh J, Hyun Park J, Scalia G, Bergström L (2014) Cellulose nanocrystal-based materials: from liquid crystal self-assembly and glass formation to multifunctional thin films. Npg Asia Mater 6:e80

Li Y, Jun-Yan Suen J, Prince E, Larin EM, Klinkova A, Therien-Aubin H, Zhu S, Yang B, Helmy AS, Lavrentovich OD et al (2016) Colloidal cholesteric liquid crystal in spherical confinement. Nat Commun 7:12520

Li C, Evans J, Wang N, Guo T, He S (2019) pH dependence of the chirality of nematic cellulose nanocrystals. Sci Rep 9:11290

Liu Q, Campbell MG, Evans JS, Smalyukh II (2014) Orientationally ordered colloidal co-dispersions of gold nanorods and cellulose nanocrystals. Adv Mater 26:7178–7184

Martin JD, Keary CL, Thornton TA, Novotnak MP, Knutson JW, Folmer JC (2006) Metallotropic liquid crystals formed by surfactant templating of molten metal halides. Nat Mater 5:271

Moon RJ, Martini A, Nairn J, Simonsen J, Youngblood J (2011) Cellulose nanomaterials review: structure, properties and nanocomposites. Chem Soc Rev 40:3941–3994

Parker RM, Guidetti G, Williams CA, Zhao T, Narkevicius A, Vignolini S, Frka-Petesic B (2018) The self-assembly of

cellulose nanocrystals: hierarchical design of visual appearance. Adv Mater 30:1704477

Schütz C, Agthe M, Fall AB, Gordeyeva K, Guccini V, Salajková M, Plivelic TS, Lagerwall JPF, Salazar-Alvarez G, Bergström L (2015) Rod packing in chiral nematic cellulose nanocrystal dispersions studied by small-angle X-ray scattering and laser diffraction. Langmuir 31:6507–6513

Segal L, Creely JJ, Martin AE, Conrad CM (1959) An empirical method for estimating the degree of crystallinity of native cellulose using the X-ray diffractometer. Text Res J 29:786–794

Shafiei-Sabet S, Hamad WY, Hatzikiriakos SG (2014) Ionic strength effects on the microstructure and shear rheology of cellulose nanocrystal suspensions. Cellulose 21:3347–3359

Stroobants A, Lekkerkerker H, Odijk T (1986) Effect of electrostatic interaction on the liquid crystal phase transition in solutions of rodlike polyelectrolytes. Macromolecules 19:2232–2238

Veerman JAC, Frenkel D (1992) Phase behavior of disklike hard-core mesogens. Phys Rev A 45:5632–5648

Wang N, Ding E, Cheng R (2008) Preparation and liquid crystalline properties of spherical cellulose nanocrystals. Langmuir 24:5–8

Wöhrle T, Wurzbach I, Kirres J, Kostidou A, Kapernaum N, Litterscheidt J, Haenle JC, Staffeld P, Baro A, Giesselmann F et al (2016) Discotic liquid crystals. Chem Rev 116:1139–1241